# We are IntechOpen, the world's leading publisher of Open Access books

# Built by scientists, for scientists

**6,900**
Open access books available

**185,000**
International authors and editors

**200M**
Downloads

**154**
Countries delivered to

Our authors are among the

**TOP 1%**
most cited scientists

**12.2%**
Contributors from top 500 universities

**CLARIVATE ANALYTICS**
**BOOK CITATION INDEX**
**INDEXED**

**WEB OF SCIENCE**™

Selection of our books indexed in the Book Citation Index
in Web of Science™ Core Collection (BKCI)

## Interested in publishing with us?
Contact book.department@intechopen.com

Numbers displayed above are based on latest data collected.
For more information visit www.intechopen.com

# Reforming $CO_2$ into Fuel Using a $TiO_2$ Photocatalyst Membrane Reactor

Akira Nishimura[1] and Eric Hu[2]
*[1]Mie University*
*[2]The University of Adelaide*
*[1]Japan*
*[2]Australia*

## 1. Introduction

Due to mass consumption of fossil fuels, global warming and fossil fuels depletion have become the serious global environmental problems in the world. After the industrial revolution, the averaged concentration of $CO_2$ in the world has been increased from 280 ppmV to 387 ppmV. Therefore, it is necessary to develop new energy production technologies with less or no $CO_2$ emission. It is reported that $CO_2$ can be reformed into fuels eg. CO, $CH_4$, $CH_3OH$ and $H_2$ etc. by using $TiO_2$ as the photocatalyst under ultraviolet (UV) light illumination (Adachi et al., 1994; Anpo & Chiba, 1992; Aurian-Blajeni et al., 1980; Dey et al., 2004; Henglein & Gutierrez, 1983; Hirano et al., 1992; Inoue et al., 1979; Ishitani et al., 1993; Kaneco et al., 1999; Ogura et al., 1992; Takeuchi et al., 2001). If this technique could be applied practically, a carbon circulation system would then be established: $CO_2$ from the combustion of fuel is reformed, using solar energy, to fuels again, and true zero emission can be achieved. Many R&D works on this technology have been carried out, using $TiO_2$ particles loaded with Cu, Pd, Pt to react with $CO_2$ dissolved in solution (Adachi et al., 1994; Goren et al., 1990; Halmann et al., 1984; Hirano et al., 1992; Ibusuki, 1993; Ishitani et al., 1993; Kawano et al., 1993; Lo et al., 2007; Tseng et al., 2002; Yamashita et al., 1994). Recently, nano-scaled $TiO_2$ (Pathak et al., 2004; Qu et al., 2005; Xia et al., 2007), porous $TiO_2$ (Cecchet et al., 2006), $TiO_2$ film combined with metal (Cueto et al., 2006; Wu & Lin, 2005), and dye sensitized $TiO_2$ (Ozcan et al., 2007), are developed for this process. However, the fuel concentration in the products achieved an all the attempts so far is still to low, ranging from 10 ppmV to 1000 ppmV, to be practically useful (Adachi et al., 1994; Dey et al., 2004; Goren et al., 1990; Halmann et al., 1984; Hirano et al., 1992; Ishitani et al., 1993; Kaneco et al., 1999; Lo et al., 2007; Pathak et al., 2004; Tseng et al., 2002; Xia et al., 2007). For the fuels to be practically useful, the concentration of produced fuels should be exceed the lowest combustible concentration of each fuel. For example, for $CH_4$ and CO, 5.3 vol.% and 12.5 vol.% is required, respectively. Therefore, the big breakthrough in increasing the concentration level is necessary to advance the $CO_2$ reforming technology.

According to the calculation by the author, the mass transfer time of $10^5$ - $10^{-1}$ s is much slower than the photo reaction time of $10^{-9}$ - $10^{-15}$ s in this process. Therefore, the mass transfer is thought to be the main factor contributing to the slow photocatalytic reaction. Another reason courses the low reforming rate is the re-oxidization of the products.

Namely, due to the reaction surface covered by products, the further movement of the reactants to the reaction surface is prevented and the reverse reaction, i.e. re-oxidization, which produces $CO_2$ from $CO$ and $CH_4$, occurs. Therefore, it is desirable that the products, i.e. $CO$ and $CH_4$ are removed from the reaction surface as soon as they are produced. The reactants i.e. $CO_2$ and water vapour can then continue to react on the reaction surface, and the fuel production can be sustained under this non-equilibrium reaction condition. In other words, by removing the products away, the reaction is forced to head to one direction. The gas separation membrane is usually used in the gas separation processes like $H_2$ production from hydrocarbon, $O_2$ enrichment from the air, and $CO_2$ capture of the industrial power plants. Since the molecular diameters of reactants of $CO_2$ and water vapour are smaller than that of $CO$ and $CH_4$ ($CO_2$: 0.33 nm, water vapour: 0.28 nm, $CH_4$: 0.38 nm, $CO$: 0.38 nm) (Nakagawa, 1988), the promotion of the reaction by gas separation is thought to be possible and was attempted in this study. This is a novel approach aiming to improve $CO_2$ reforming performance over the $TiO_2$. No similar attempts have been reported yet.

Since this research approach is very novel, the following subjects are set in this study:

i.   Optimization of preparation condition, especially rising speed (*RS*) of gas separation membrane from the $TiO_2$ sol solution in dip-coating process in order to select the optimal $TiO_2$ film coating conditions to prepare the membrane for the reactor of gas circulation type,

ii.  Verification of the concept of this study which is promotion of $CO_2$ reforming performance by gas separation and circulation,

iii. Proposal of $TiO_2$ photocatalyst power system with zero $CO_2$ emission for the future.

This chapter introduces the authors' approach to research and develop the $TiO_2$ photocatalyst membrane reactor consisting of $TiO_2$ photocatalyst and gas separation membrane. At first, the preparation procedure of $TiO_2$ film coated on gas separation membrane is introduced. To optimize the preparation condition, the surface structure and crystallization characteristics of $TiO_2$ film coated on gas separation membrane are analysed. In addition, the $CO_2$ reforming and permeation performance of $TiO_2$ film coated on porous gas separation membrane is evaluated by the batch type reactor. Finally, the $CO_2$ reforming performance of $TiO_2$ film coated on porous gas separation membrane is investigated by the gas circulation type reactor and the concept of this study which is promotion of $CO_2$ reforming performance by gas separation and circulation is verified.

## 2. Research and development on TiO$_2$ photocatalyst membrane reactor

Since $TiO_2$ photocatalyst membrane reactor is a novel approach to improve $CO_2$ reforming performance over the $TiO_2$, it is necessary to verify the effect of combination of gas separation membrane and $TiO_2$ on $CO_2$ reforming performance. Therefore, the authors investigated the preparation procedure of $TiO_2$ film coated on gas separation membrane by sol-gel and dip-coating method and the experimental operation conditions to promote the $CO_2$ reforming performance of the $TiO_2$ photocatalyst membrane reactor. The *RS* which influences the thickness and physical and chemical structure of $TiO_2$ film coated on gas separation membrane was investigated. The surface structure and crystallization characteristics of $TiO_2$ film coated on gas separation membrane, under the various *RS* conditions, were analysed by SEM (Scanning Electron Microscope), EPMA (Electron Probe Micro Analyzer) and XPS (X-ray Photoelectron Spectroscopy) to understand the impact of difference of *RS* on the surface structure and crystallization characteristics of $TiO_2$ film, as

the first step. The CO$_2$ reforming and permeation performance of TiO$_2$ film coated on gas separation membrane was evaluated by the batch type reactor in order to select the optimal TiO$_2$ film coating conditions to prepare the membrane for the reactor of gas circulation type. In other words, the ideal TiO$_2$ film for this application should have large reaction surface areas and high crystallization characteristics but does not block the pores in gas separation membrane. After the suitable TiO$_2$ film coating conditions are known, the CO$_2$ reforming performance of TiO$_2$ film coated on porous gas separation membrane was investigated by the gas circulation type reactor. The effectiveness of gas separation and gas circulation using the gas separation membrane on CO$_2$ reforming performance was compared with the results obtained from the batch type reactor experiment.

## 2.1 Preparation of TiO$_2$ film coated on gas separation membrane

Sol-gel and dip-coating method was used for preparing TiO$_2$ film in this study. Figure 1 shows the flow chart of the sol-gel and dip-coating method. TiO$_2$ sol solution was made by mixing [(CH$_3$)$_2$CHO]$_4$Ti (purity of 95 wt.%, Nacalai Tesque Co.), anhydrous C$_2$H$_5$OH (purity of 99.5 wt.%, Nacalai Tesque Co.), distilled water, and HCl (purity of 35 wt.%, Nacalai Tesque Co.).
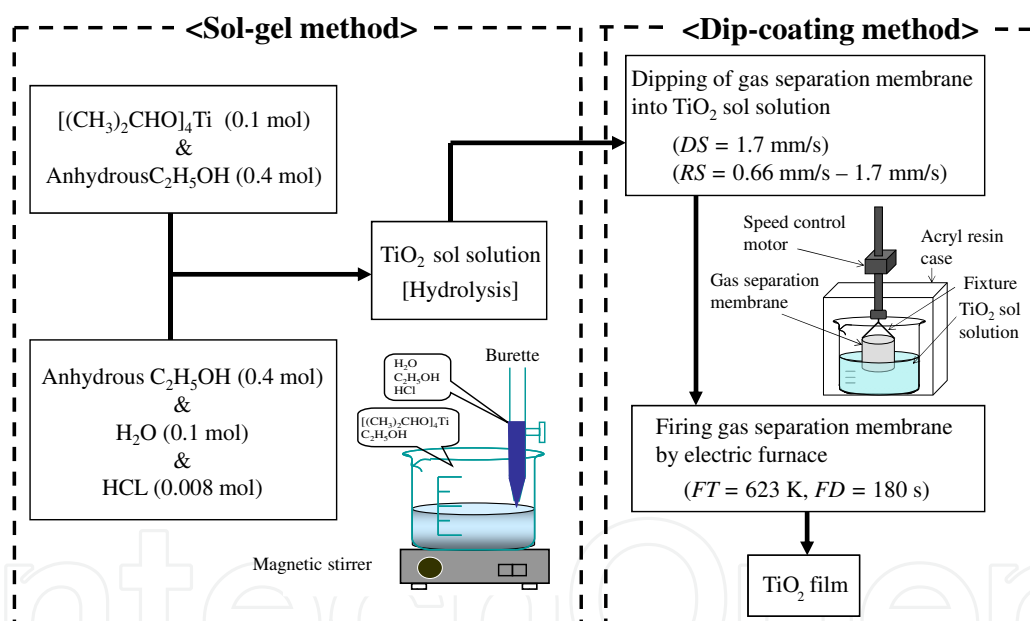


Fig. 1. Sol-gel and dip-coating method to prepare TiO$_2$ film in this study

The gas separation membrane (silica-alumina gas separation membrane, Noritake Co., Ltd.), which was the porous multilayer ceramic tube shown in Fig.2, was dipped into TiO$_2$ sol solution and pulled up at the fixed speed. Then, it was dried out and fired under the controlled firing temperature (*FT*) and firing duration time (*FD*), resulting that TiO$_2$ film was fastened on the surface of gas separation membrane. Coating number (*N*) was fixed at 1. *FT* and *FD* was set at 623 K and 180 s, respectively. *RS* varied from 0.66 mm/s to 1.7 mm/s. Downing speed (*DS*) of gas separation membrane into TiO$_2$ sol solution in dip-coating process was kept at the constant speed of 1.7 mm/s. Table 1 lists the physical properties of the gas separation membrane. It can be seen from Table 1, the mean pore size of silica layer is not ideal, as it is not between the molecular diameter of reactants and that of

products, as required. It is difficult to find the gas separation membrane with the ideal pore size. However, the gas separation membrane selected is capable of separating gases through both molecular sieving diffusion and so called Knudsen diffusion mechanisms, therefore it can be used. The Knudsen diffusion can separate the gases whose molecular diameters are smaller than the pore size of silica layer. Since the molecular diameter of reactant and that of product is actually different as described above, we have decided to adopt this gas separation membrane.



Fig. 2. Gas separation membrane

| | Thickness (μm) | Mean pore size (nm) | Void ratio (-) | Permeability (m$^2$) |
|---|---|---|---|---|
| 1. Silica (SiO$_2$) layer | 0.2 | 0.4 | 0.27 | $5.44 \times 10^{-22}$ |
| 2. γ-alumina (Al$_2$O$_3$) layer | 2 | 4 | 0.44 | $8.88 \times 10^{-20}$ |
| 3. α-alumina (Al$_2$O$_3$) layer | 100 | 60 | 0.39 | $1.76 \times 10^{-17}$ |
| 4. α-alumina (Al$_2$O$_3$) supporter | 1000 | 700 | 0.40 | $2.45 \times 10^{-15}$ |
| Silica layer is the top layer of this gas separation membrane. | | | | |
| γ-alumina layer is the second layer. α-alumina layer is the third layer. | | | | |
| α-alumina supporter is the bottom layer of gas separation membrane. | | | | |

Table 1. Physical properties of gas separation membrane

### 2.1.1 Analysis result of TiO$_2$ film coated on gas separation membrane by SEM

Figures 3 and 4 show SEM images of TiO$_2$ film prepared under various *RS* conditions. These SEM images were taken with 200 times and 1500 times magnification under the condition of acceleration voltage of 15 kV and current of $3.0 \times 10^{-8}$ A. The silica layer covers one third of surface area of gas separation membrane used in this study at the center and the alumina layer is exposed except for the area covered by silica layer. Then, SEM images of TiO$_2$ film coated were taken for the silica covered area and the alumina area separately. From these figures, it can be seen that the number of clucks of TiO$_2$ film coated on alumina layer is less than that on silica layer, resulting that the amount of TiO$_2$ coated on alumina layer is larger than silica layer. Since the pore size of alumina layer is larger than that of silica layer as listed in Table 1, it can be thought that TiO$_2$ sol solution flows into the alumina layer more

easily than the silica layer in dip-coating process. Therefore, it seems that TiO$_2$ film coated on alumina layer is fixed more strongly than that on silica layer.
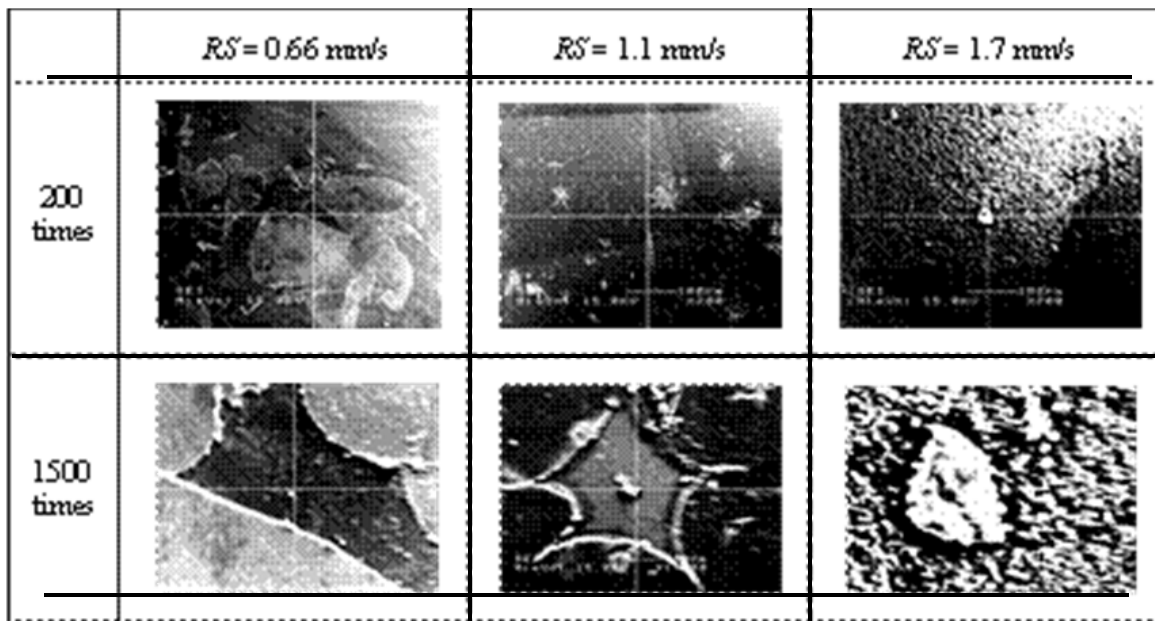


Fig. 3. SEM images of TiO$_2$ film coated on silica layer prepared under various *RS* conditions
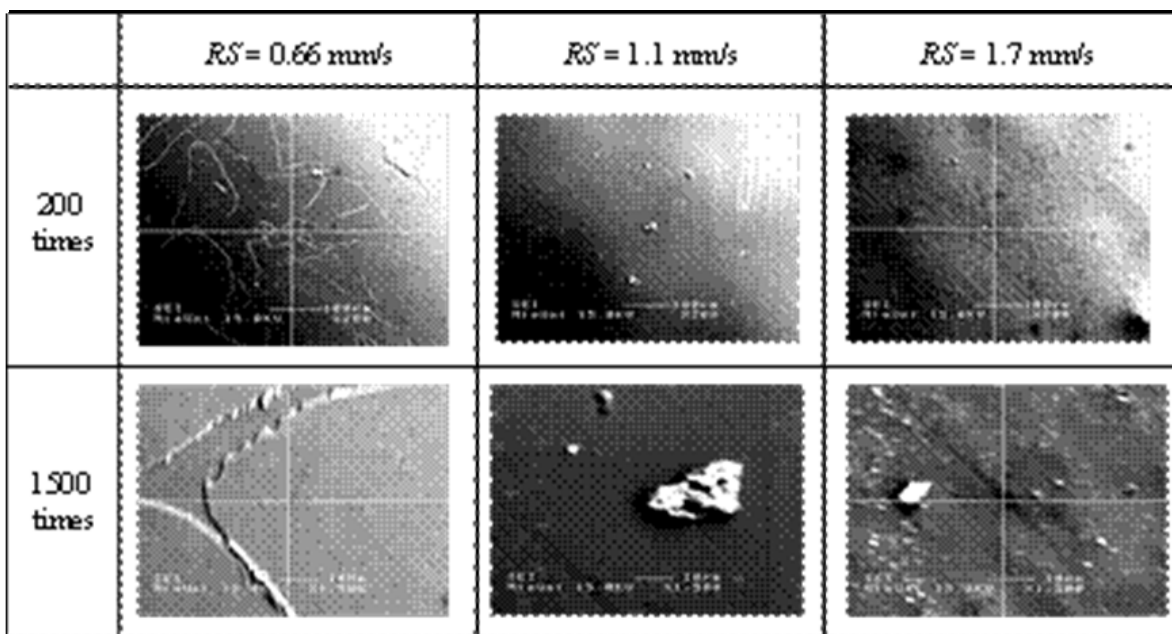


Fig. 4. SEM images of TiO$_2$ film coated on alumina layer prepared under various *RS* conditions

### 2.1.2 Analysis result of TiO₂ film coated on gas separation membrane by EPMA

Figure 5 demonstrates EPMA images of TiO$_2$ film prepared under various *RS* conditions. These EPMA images are taken by 1500 times magnification under the condition of acceleration voltage of 15 kV and current of $3.0 \times 10^{-8}$ A. Tables 2 and 3 list the distribution of Ti concentration detected for silica layer and alumina layer, respectively.

| | RS = 0.66 mm/s | RS = 1.1 mm/s | RS = 1.7 mm/s |
|---|---|---|---|
| Silica layer | | | |
| Average [cps] | 1 | 0 | 0 |
| Alumina layer | | | |
| Average [cps] | 2 | 2 | 0 |
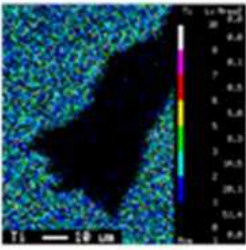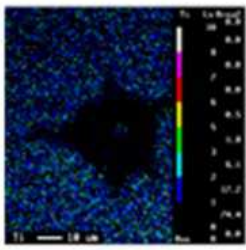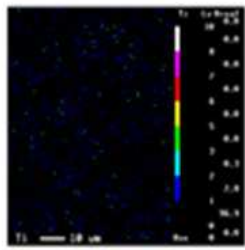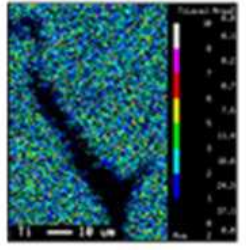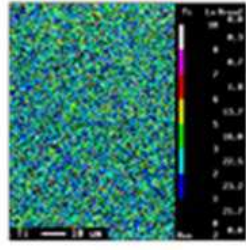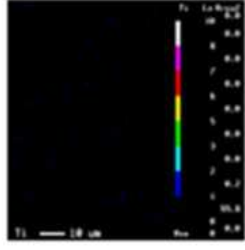
Fig. 5. EPMA images of TiO$_2$ film prepared under various *RS* conditions

| | $RS = 0.66$ mm/s | $RS = 1.1$ mm/s | $RS = 1.7$ mm/s |
|---|---|---|---|
| Concentration of detected Ti (cps) | | | |
| 10 | 0 | 0 | 0 |
| 10~8 | 0 | 0 | 0 |
| 8~7 | 0.1 | 0 | 0 |
| 7~6 | 0.5 | 0 | 0 |
| 6~5 | 5.0 | 0.5 | 0 |
| 5~3 | 8.3 | 1.8 | 0 |
| 3~2 | 14.5 | 6.1 | 0.3 |
| 2~1 | 20.1 | 17.2 | 2.8 |
| 1~0 | 51.4 | 74.4 | 96.9 |
| 0 | 0 | 0 | 0 |

Table 2. Concentration distribution of Ti detected by EPMA (silica layer)

| Concentration of detected Ti (cps) | $RS$ = 0.66 mm/s | $RS$ = 1.1 mm/s | $RS$ = 1.7 mm/s |
|---|---|---|---|
| 10 | 0 | 0 | 0 |
| 10~8 | 0.1 | 0.3 | 0 |
| 8~7 | 0.2 | 0.7 | 0 |
| 7~6 | 0.7 | 1.8 | 0 |
| 6~5 | 7.5 | 13.7 | 0 |
| 5~3 | 11.4 | 16 | 0 |
| 3~2 | 18.6 | 22.5 | 0 |
| 2~1 | 24.3 | 23.2 | 0.2 |
| 1~0 | 37.1 | 21.7 | 99.8 |
| 0 | 0 | 0 | 0 |

Table 3. Concentration distribution of Ti detected by EPMA (alumina layer)

In Fig.5, the concentration distribution of Ti detected in observation area is indicated by the difference of colour. Light colours, e.g. white, pink and red mean that the amount of Ti is large, while dark colours like black, blue and green mean that the amount of Ti is small. EPMA detects the each element whose crystallization characteristic is memorized in advance. Therefore, if the large concentration of Ti is detected, it means that the amount of crystallized TiO₂ coated on gas separation membrane is large. The average concentration of Ti in the observation area is also shown in Fig.5. According to Fig.5, the average concentration of Ti detected in observation area for alumina layer is larger than that for silica layer. It can be said that TiO₂ film is coated in the pores of alumina layer mainly. From Fig.5, Tables 2 and 3, it reveals that the concentration of Ti is reduced with the increase in $RS$. Generally speaking, the thickness of TiO₂ film becomes thick and hubbly with the increase in $RS$. The thermal stress is acted on the interface between TiO₂ film and gas separation membrane in the firing process, resulting that formation of large clucks and detachment of TiO₂ film occur. Consequently, the concentration of Ti is reduced when $RS$ is high.

### 2.1.3 Analysis result of TiO₂ film coated on gas separation membrane by XPS

Figures 6 and 7 show the intensity distributions of Ti detected in silica layer and alumina layer, respectively. These XPS data were obtained under the condition of ion acceleration voltage of 4 kV and pass energy of 112 eV. The samples were sputtered by Ar ion laser whose acceleration voltage of 2 kV. The sputtering speed was 15 nm/min, which was estimated by assuming the sample as SiO₂. The electron orbits of detected elements which were Ti, Si and Al were set at 2p. From these figures, it is known that the sputtering time of $RS$ = 1.1 mm/s is the shortest among various $RS$ conditions. However, the intensity of detected Ti is over 80000 cps for $RS$ = 1.1 mm/s. It can be said that the amount of Ti is large with $RS$ = 1.1 mm/s, resulting that fine TiO₂ film is prepared. Regarding $RS$ = 0.66 mm/s, it is seen that the intensity of Ti over 60000 cps can be detected up to about sputtering time of 25 min for silica layer. Though the intensity of Ti detected in alumina layer is smaller than

that in silica layer, the detecting period of Ti in alumina layer is almost equal to that in silica layer. According to Fig.5, the average concentration of Ti for $RS$ = 0.66 mm/s is the largest
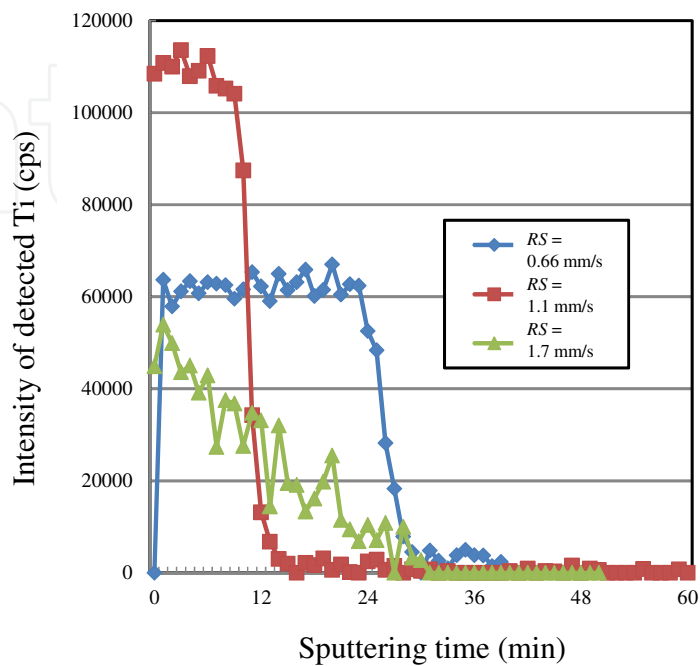
Fig. 6. Intensity distributions of detected Ti in silica layer
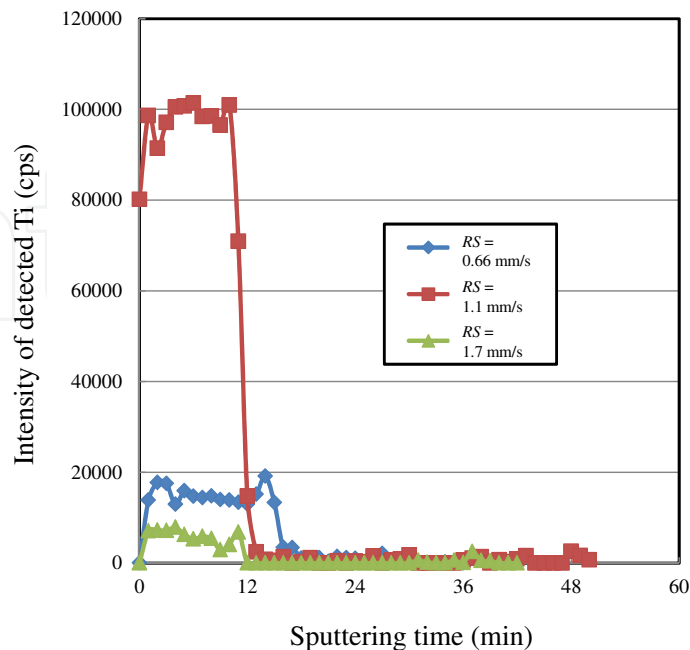
Fig. 7. Intensity distributions of detected Ti in alumina layer

among various *RS* conditions. From these results, one can conclude that the largest amount of TiO$_2$ film is coated on gas separation membrane with *RS* = 0.66 mm/s. Meanwhile, the intensity of detected Ti with *RS* = 1.7 mm/s is the lowest among various *RS* conditions. In addition, the average concentration of Ti is 0 cps as shown in Fig.5. Consequently, it is clear that the amount of TiO$_2$ film coated on gas separation membrane for *RS* = 1.7 mm/s is very small.

## 2.2 Performance of TiO₂ photocatalyst membrane reactor under batch type operation

Figure 8 illustrates the CO$_2$ reforming reactor that is termed as CO$_2$ reformer, with TiO$_2$ film coated on gas separation membrane. This reactor consists of one gas separation membrane with TiO$_2$ film (150 mm (*L.*)×6 mm (*O.D.*)×1 mm (*t.*), whose reaction surface is equal to the outer surface area: $2.26 \times 10^{-3}$ m$^2$ and gas filling volume: $2.88 \times 10^{-4}$ m$^3$) , one quartz glass tube (266 mm (*L.*)×42 mm (*O.D.*)×2 mm (*t.*)), and four UV lamps (FL16BL/400T16, Raytronics Corp., 400 mm (*L.*)×16 mm (*D.*)) located at 20 mm apart from the surface of gas separation membrane symmetrically. These parts are assembled with stainless plates by bolts and nuts. The center wave length and mean light intensity of UV light illuminated from energy UV lamp is 365 nm and 2.4 mW/cm$^2$, respectively. This is similar to the average light intensity level of UV ray in solar radiation in the daytime.
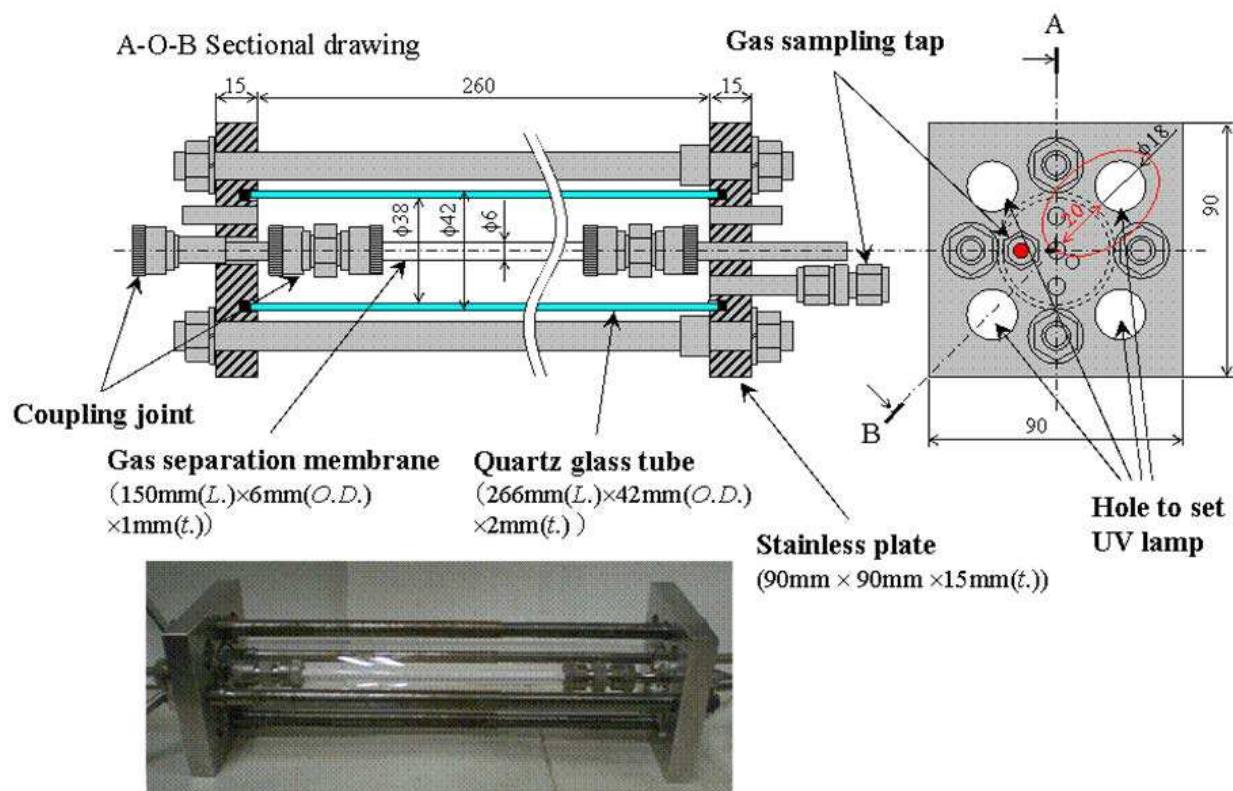


Fig. 8. CO$_2$ reformer composed of TiO$_2$ film coated on gas separation membrane (UV lamp is removed from this figure for understanding the inside of CO$_2$ reformer)

(1) $CO_2$ gas cylinder            (2) Regulator
    (99.995 vol%)

(3) Mass flow controller         (4) Pressure gauge

(5) $CO_2$ reformer               (6) Dew point meter

(7) Thermocouple                  (8) Gas drier (Silica gel)

(9) Mass flow meter               (10) Tube pump
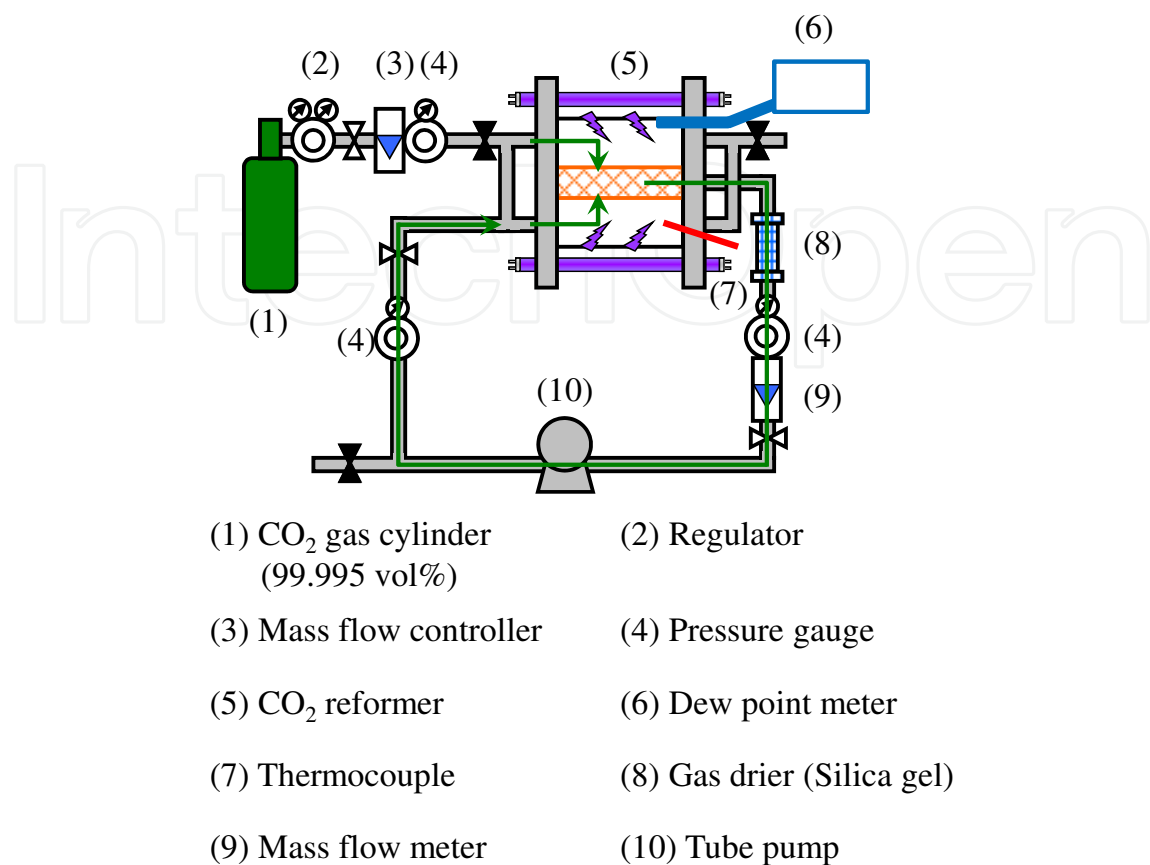
Fig. 9. $CO_2$ reforming and permeation experiment system

Figure 9 illustrates the whole experimental system set-up, which is termed as membrane reactor. With this membrane reactor, not only batch type but also gas circulation type experiment can be conducted. When it is used for batch type experiment, the valves located at inlet and outlet of $CO_2$ reformer are closed. The membrane reactor is composed of $CO_2$ reformer, $CO_2$ gas cylinder, mass flow controller (MODEL3660, KOFLOC), mass flow meter (CK-1A, KOFLOC), pressure gauge, gas drier and tube pump (WM-520S/R2, Iwaki Pumps). In the $CO_2$ reforming experiment by the batch type reactor, $CO_2$ gas whose purity was 99.995 vol.% was flowed through the $CO_2$ reformer as a purged gas for 15 min at first. After that, the valves located at inlet and outlet of $CO_2$ reformer were closed. After confirming the gas pressure and gas temperature in the reactor was at 0.1 MPa and 298 K, respectively, the distilled water of 1.00 mL (55.6 mmol) was injected into the $CO_2$ reformer and UV light illumination was started at the same time. This water was vaporized after injected into the reformer. Despite the heat of UV lamp, the temperature in $CO_2$ reformer was kept at about 343 K during the $CO_2$ reforming experiment. The amounts of the injected water and the $CO_2$ in the batch type reactor are 55.6 mmol and 13.0 mmol, respectively. The gas in $CO_2$ reformer was sampled every 24 h in $CO_2$ reforming experiment. The gas samples were analysed by FID gas chromatograph (GC353B, GL Science) and methanizer (MT221, GL Science). The concentration of water vapour and the temperature in $CO_2$ reformer was measured by dew point meter (VAISALA HUMICAP HMT330, VAISALA) and thermocouple, respectively. In this experiment, only CO was detected as the product. In the

$CO_2$ permeation experiment, the $CO_2$ reforming and permeation experimental system shown in Fig.9 was arranged.



(1) $CO_2$ gas cylinder     (2) Regulator     (3) Mass flow controller

(4) Pressure gauge     (5) Gas separation membrane     (6) Pressure gauge

(7) Mass flow meter
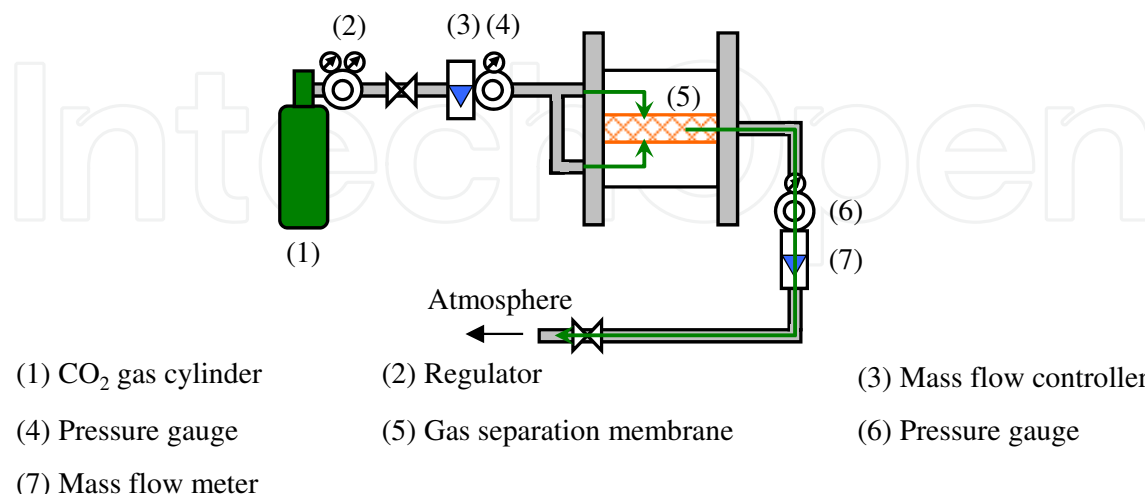
Fig. 10. Arranged $CO_2$ reforming and permeation experimental system for $CO_2$ permeation experiment

Figure 10 illustrates the $CO_2$ reforming and permeation experimental system for $CO_2$ permeation experiment by batch type. In the $CO_2$ permeation experiment, the $CO_2$ permeation flux was measured under the condition that the absolute pressure and temperature of supply gas to the apparatus was 0.10-0.40 MPa and 298 K, respectively. The flow rate of supply gas was set at 500 mL/min by mass flow controller. The flow rate of permeation gas was measured by mass flow meter. In the $CO_2$ reforming experiment carried out by the membrane reactor of gas circulation type, UV light was illuminated under the same condition of batch type reactor until the steady reaction state was confirmed. After that, the gas circulation by tube pump was started. The suction pressure and flow rate of permeation gas was controlled to evaluate the effect of gas separation and circulation on $CO_2$ reforming performance of this membrane reactor. The suction pressure and flow rate of permeation gas was set at 0.2 MPa and 0.39 mL/min, respectively. The produced CO would be removed from the $CO_2$ reformer to outside of the system by switching the outlet valve of $CO_2$ reformer on and off when needed. The distilled water of 1.00 mL (55.6 mmol) or 3.00 mL (166.8 mmol) was injected into $CO_2$ reformer when the $CO_2$ reforming experiment under the condition of batch type reactor was established. The gas samples taken every 24 h from $CO_2$ reformer were analysed by FID gas chromatograph and methanizer. The concentration of water vapour and the temperature in the $CO_2$ reformer were also measured.

### 2.2.1 $CO_2$ reforming by the membrane reactor of batch type

Figure 11 shows the CO concentration change in products with illumination time of UV light for several $TiO_2$ films prepared under various *RS* conditions. According to our

previous studies, the reversal of superiority or inferiority on $CO_2$ reforming performance of $TiO_2$ film among selected parameters was confirmed until UV light illumination time of 48 h. However, this reversal was not confirmed and the superiority or inferiority among selected parameters was kept after UV light illumination time of 72 h. From this reason, in this study, the data is obtained only up to UV light illumination time of 72 h for the purpose of determining the best condition for promotion of $CO_2$ reforming performance. The distilled water of 1.00 mL (55.6 mmol) was injected into $CO_2$ reformer at the beginning of the $CO_2$ reforming experiment.
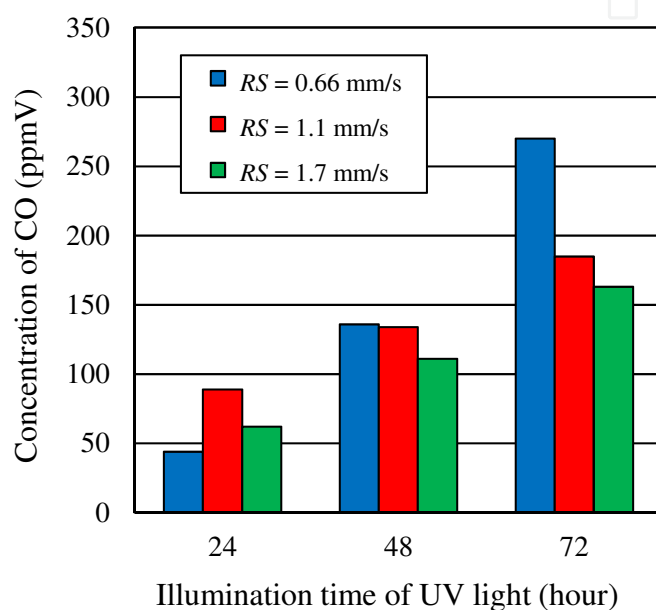


Fig. 11. Concentration change in produced CO with illumination time of UV light for several $TiO_2$ film prepared under conditions of different *RS*

From Fig.11, it is known that the concentration of CO is increased with decreasing *RS* values. Referring to the images of the SEM, EPMA and XPS shown in Figs.3, 4, 5, 6 and 7, the reason of this is thought to be that the amount of $TiO_2$ coated on gas separation membrane becomes larger when *RS* decreases within the range of 0.66 – 1.7 mm/s. Under slow *RS* condition, $TiO_2$ sol solution is easy to remain in the pore of silica and alumina layer in the dip-coating process, and $TiO_2$ film coated becomes thin and even. Consequently, the fine and strong $TiO_2$ film is prepared.

According to the reaction scheme shown in Fig.12, the number of electron and hydrogen ion ($H^+$) decides the type of product in the reaction. In this experiment, $CH_4$, $C_2H_4$ and the other hydrocarbons were not detected by gas chromatograph, due to less $H^+$ in the reaction. Therefore, the amount of water vapour injected into the reactor is an important parameter to be investigated since it is the source of $H^+$. From the reaction scheme, water vapour of 1 mol to $CO_2$ of 1 mol is necessary to produce CO of 1 mol. In this experiment, the amount of substance of injected water and $CO_2$ charged in the batch type reactor is 55.6 mmol and 13.0 mmol, respectively, resulting that the molar ratio of water vapour to

$CO_2$ is 4.28. Although the amount of water vapour injected seemed sufficient for this reaction, the change in temperature distribution and the concentration distribution of water vapour in the batch type reactor with time need to be checked to confirm what had happened.

**<Photocatalytic Reaction>**

$$TiO_2 + h\nu \text{ (under 380 nm)} \rightarrow h^+ + e^-$$

**<Oxidation>**

$$H_2O \xrightarrow{h^+} \cdot OH + H^+$$

$$\cdot OH + H_2O \xrightarrow{h^+} O_2 + 3H^+$$

**<Reduction>**

$$CO_2 \xrightarrow[H_2O]{2H^+ + 2e^-} CO \xrightarrow[H_2O]{4H^+ + 4e^-} \cdot CH_2$$

$$\cdot CH_2 \xrightarrow{2H^+ + 2e^-} CH_4$$

$$\xrightarrow{\cdot CH_2} C_2H_4$$

$$\xrightarrow{\cdot CH_2 + 2H^+ + 2e^-} C_2H_6$$

Fig. 12. Reaction scheme of $CO_2$ reforming into fuel by $TiO_2$ photocatalyst

Figure 13 shows the concentration change of water vapour in $CO_2$ reformer with illumination time of UV light during $CO_2$ reforming for several $TiO_2$ films prepared under various *RS* conditions. From this figure, it can be known that the concentration of water vapour for *RS* = 0.66 mm/s is the smallest among several *RS* conditions during UV light illumination from 0 h to 24 h. Under the same conditions, the temperatures in $CO_2$ reformer rose up to about 343 K during UV light illumination from 0 h to 24 h, and then remained steady irrespective of *RS*. The water injected had fully evaporated by UV light illumination at the time of 24 h. The reason why the concentration of water vapour for *RS* = 0.66 mm/s is the smallest can be explained by the results of XPS analysis. According to the results of XPS analysis, the largest amount of $TiO_2$ film is coated on gas separation membrane for *RS* = 0.66 mm/s, and the $TiO_2$ film is coated deeply to thickness direction in the pores of silica and alumina layer. The $CO_2$ reforming is carried out well and consumes more water, compared to the other *RS* conditions in the oxidization process of the reaction scheme. Therefore, the concentration of water vapour and CO for *RS* = 0.66 mm/s becomes low during the period from 0 h to 24 h, and the concentration of CO for

$RS$ = 0.66 mm/s is the largest among the investigated $RS$ conditions as shown in Fig.11. Although the water is produced in the reduction process of $CO_2$ reforming by $TiO_2$, this water vapour seems to be adsorbed by $TiO_2$ film or gas separation membrane. Therefore, the concentration of water vapour did not increase irrespective of $RS$ as shown in Fig.13. According to saturated steam table, the saturation concentration of water vapour at 343 K is 307545 ppmV, while the 55.6 mmol of water injected, if all evaporates, just makes the concentration of 53040 ppmV in $CO_2$ reformer theoretically. Therefore, the all of water injected in $CO_2$ reformer is thought to be vaporized. On the contrary, the measured concentration of water vapour obtained in $CO_2$ reforming is just 25000 ppmV as shown in Fig.13. The gap between theoretical and experimental results might be caused by water vapour adsorption with $TiO_2$ film and gas separation membrane in the experiment of $CO_2$ reforming.



Illumination time of UV light (hour)
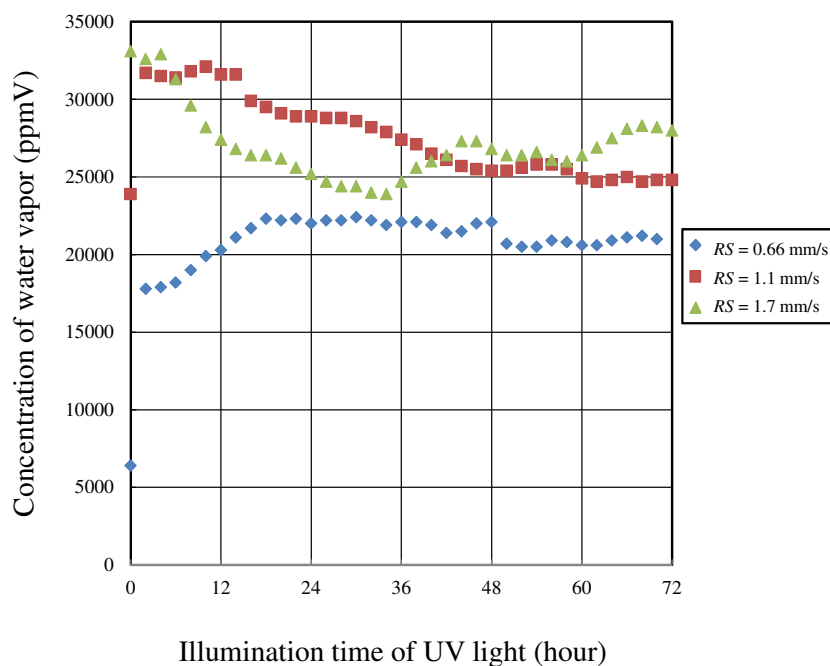
Fig. 13. Concentration change of water vapour in $CO_2$ reformer with illumination time of UV light during $CO_2$ reforming for several $TiO_2$ films prepared under various $RS$ conditions

### 2.2.2 $CO_2$ permeation by the membrane reactor of batch type

Figure 14 shows the relationship between $CO_2$ permeation flux and pressure difference for several $TiO_2$ film prepared under various $RS$ conditions. The pressure difference is known by subtracting the gas pressure after penetrating the gas separation membrane from the gas pressure before. The $CO_2$ permeation flux is calculated by the following equation:

$$F_{CO_2} = \frac{V_p}{A_p t_p}$$ (1)

where $F_{CO_2}$, $V_p$, $A_p$ and $t_p$ are $CO_2$ permeation flux (mol/(m²·s)), volume of permeated gas (mol), outer surface area of gas separation membrane (m²) and gas separation time (s), respectively.
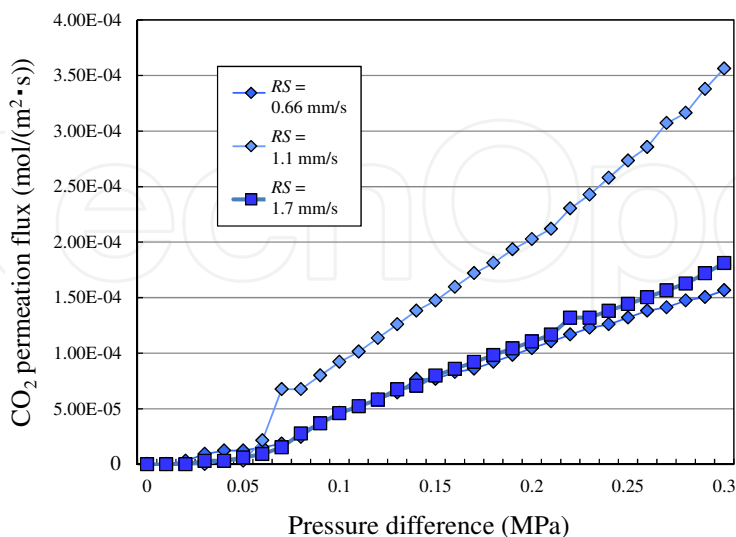
Fig. 14. Relationship between CO$_2$ permeation flux and pressure difference for several TiO$_2$ film prepared under various *RS* conditions

Comparing these results at pressure difference of 0.30 MPa, it is known that the CO$_2$ permeation flux for *RS* = 1.1 mm/s is the highest among these *RS* conditions. According to XPS analysis as shown in Figs. 6 and 7, the sputtering time of detecting Ti for *RS* = 1.1 mm/s is the shortest among various *RS* conditions, indicating that the depth of coated TiO$_2$ film diffused into the silica and alumina layers of gas separation membrane is the shallowest. Consequently, the highest CO$_2$ permeation flux is obtained at *RS* = 1.1 mm/s. On the other hand, regarding *RS* = 0.66 mm/s and 1.7 mm/s, the sputtering time of detecting Ti is longer though the intensity of Ti detected is lower as shown in Figs. 6 and 7, indicating the depth of coated. TiO$_2$ film diffused into the silica and alumina layers is deeper, thus the CO$_2$ permeation flux is lower.

### 2.2.3 Selection of the optimum coating condition

To select the optimum coating condition of TiO$_2$ film which would lead to the highest CO$_2$ reforming and permeation performance, the results by SEM and EPMA analysis and the results of CO$_2$ reforming and permeation experiment by the batch type reactor are compared and analysed. Figure 15 shows the comparison of the results between the concentration of produced CO and the CO$_2$ permeation flux for various *RS* conditions. In Fig.15, the concentration of CO at UV illumination of 72 h and CO$_2$ permeation flux at pressure difference of 0.30 MPa are shown. It can be seen that the concentration of CO is decreased with increasing *RS* gradually. On the other hand, the CO$_2$ permeation flux peaks at *RS* = 1.1 mm/s. Therefore, the optimum *RS* is different from the viewpoint of CO$_2$ reforming and permeation performance. Since the main goal of this study is to promote the CO$_2$ reforming performance, we have selected the *RS* = 0.66 mm/s as the optimum coating condition.
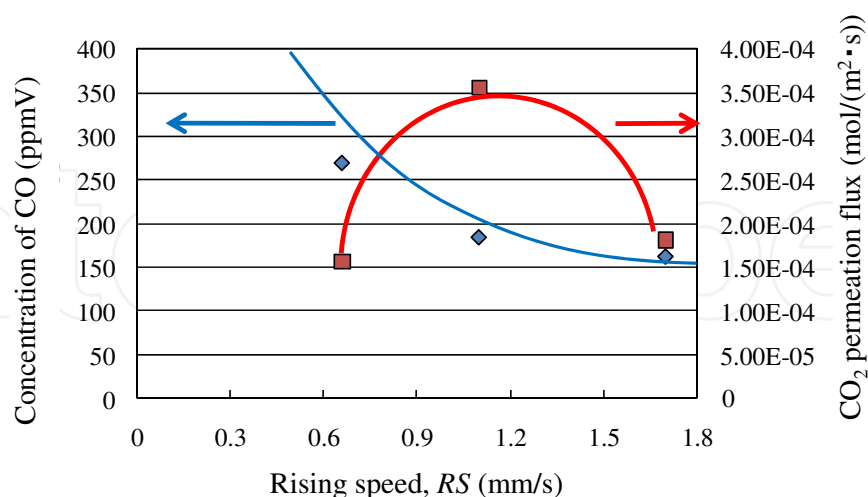
Fig. 15. Comparison of the results between concentration of produced CO and $CO_2$ permeation flux for each condition

## 2.3 Performance of TiO$_2$ photocatalyst membrane reactor under gas circulation type operation

According to the reaction scheme shown in Fig.12, CO is re-oxidized with the $O_2$ that is a by-product in this reaction. After attaining to the steady reaction state, the concentration of CO is decreased. This is the opposite reaction toward $CO_2$ reforming into fuel. Moreover, since the photocatalytic reaction occurred on the reaction surface, it is easy for the reaction surface to be covered by the products, which would stop the further reaction to happen. Therefore, removing the product of CO and CH$_4$ from the reaction surface as well as transporting the reactants, i.e. $CO_2$ and water vapour to the reaction surface quickly are necessary to promote further reaction and prevent the re-oxidization of CO. In this study, a tube pump and a gas separation membrane are used to realize this desirable measure for the promotion of $CO_2$ reforming performance.

### 2.3.1 CO$_2$ reforming by the membrane reactor of gas circulation type

Figure 16 shows the concentration change of CO produced with illumination time of UV light. The distilled water of 1.00 mL (55.6 mmol) was injected into $CO_2$ reformer when the $CO_2$ reforming experiment by batch type reactor started. To show the effect of gas separation and circulation on the $CO_2$ reforming performance, the gas circulation by tube pump only starts after the steady reaction state is reached. The steady reaction state was defined as the state at which the concentration of CO no longer increases along the time. Since the concentration of CO is diluted with the $CO_2$ in the pipe lines of the gas circulation type reactor after starting gas circulation, the concentration of CO is corrected by the following equation:

$$C_c = \frac{V_{total} C_d}{V_{batch}} \tag{2}$$

where $C_c$, $V_{total}$, $C_d$ and $V_{batch}$ means corrected concentration of CO (ppmV), total gas volume inside the experimental apparatus including the gas volume in the pipe lines (m³), detected concentration of CO (ppmV), and total gas volume inside the experimental apparatus in the case of batch type reactor (m³), respectively. The experiment by batch type and gas circulation type was carried out during the period from 0 h to 216 h and from 216 h to 480 h, respectively.
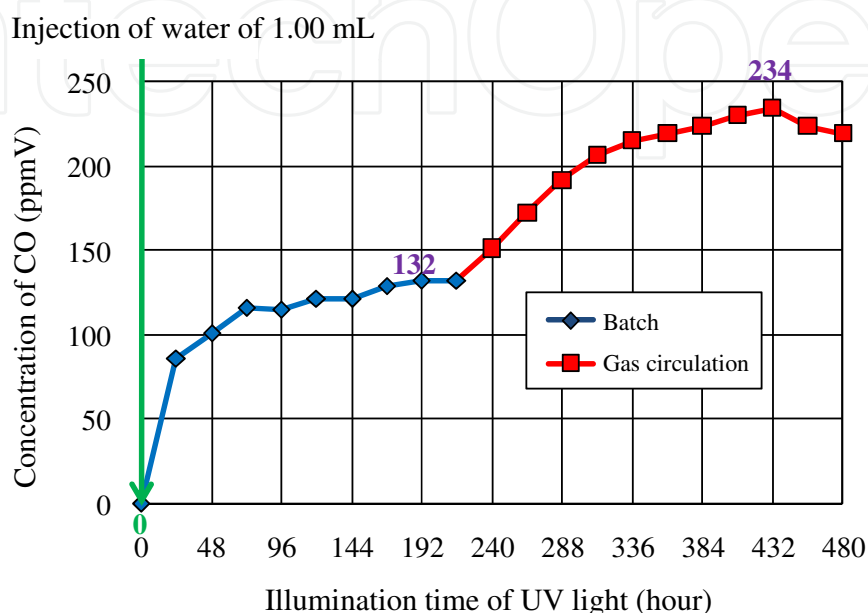


Fig. 16. Concentration change in produced CO with illumination time of UV light (Injection of water of 1.00 mL at the start of CO₂ reforming experiment)

It is observed that the concentration of CO in the reactor keeps increasing until 72 h and starts to be steady after 72 h in the experiment by batch type reactor. The highest concentration of CO which is 132 ppmV is obtained at 192 h after illuminating UV light. Since the concentration of CO is not increased over 192 h, it is determined that the experiment by batch type reactor reaches the steady reaction state at 192 h. After gas circulation, the concentration of CO starts to increase again, and peaks at 234 ppmV at UV light illumination of 432 h, which demonstrated the positive effect of gas separation and circulation on CO₂ reforming performance. To show that the steady reaction state and inverse reaction have occurred or not clearly, the change in production rate of CO with illumination time of UV light is shown in Fig.17. Production rate of CO can classify the reaction state into progressive, steady and inverse reaction state by positive, 0 and negative value, respectively. The production rate of CO, in Fig.17, which is calculated by Eq. (3):

$$R_{CO} = \frac{C_C}{t_{int}} \tag{3}$$

where $R_{CO}$ and $t_{int}$ means production rate of CO (ppmV) and gas sampling interval (h), respectively. The $R_{CO}$ used for calculating is 24 h.
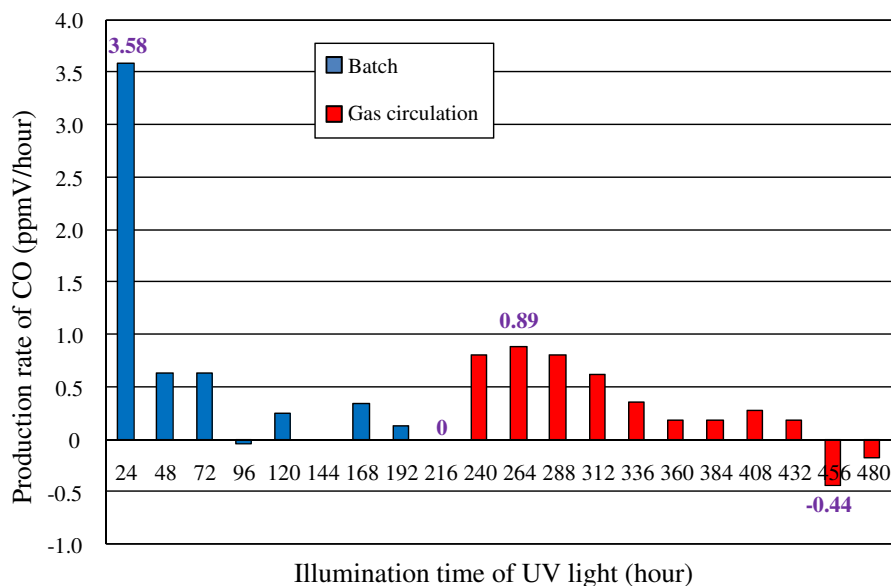
Fig. 17. Change in production rate of CO with illumination time of UV light (Injection of water of 1.00 mL at the start of $CO_2$ reforming experiment)

In the experiment by batch type reactor, it can be seen that the production rate of CO peaks at 3.58 ppmV/h at the UV light illumination time of 24 h and is decreased afterwards gradually. The production rate of CO which is 0 means the reaction steady state is reached. The negative value of the production rate means the inverse reaction, i.e. re-oxidization occurs. In the experiment by gas circulation type reactor, the production rate of CO after starting the gas circulation peaks at the highest value of 0.89 ppmV/h in the period from 240 h to 264 h. However, the production rate of CO became smaller after the passage time of 48 h, i.e. after the total illumination time of UV light of 264 h. Comparing the production rate of CO after starting the gas circulation and that at steady state of batch type reactor except for the period from 0 h to 24 h, the effect of gas separation and circulation on $CO_2$ reforming can be verified. However, the production rate of CO and the concentration of CO are still lower than the target value levels set for this study. Figure 18 shows the concentration of the water vapour during the $CO_2$ reforming experiment by batch type and gas circulation type reactor with illumination time of UV light. Since the concentration of water vapour is diluted with the gas in the pipe lines of the gas circulation type reactor after starting gas circulation, the concentration of water vapour is corrected by the following equation:

$$C_{c-H2O} = \frac{V_{total}C_{d-H2O}}{V_{batch}}$$

(4)

where $C_{c-H2O}$, $V_{total}$, $C_{d-H2O}$ and $V_{batch}$ means corrected concentration of water vapour (ppmV), total gas volume inside the experimental apparatus including the gas volume in the pipe lines ($m^3$), measured concentration of water vapour (ppmV), and total gas volume inside the experimental apparatus in the case of batch type reactor ($m^3$), respectively. From this figure, it is known that the highest concentration of water vapour

in the experiment by batch type reactor and gas circulation reactor is 32400 ppmV and 65387 ppmV, respectively. As described above, if the water vapour is saturated in the reactor at 343 K, it should have the concentration of 307545 ppmV. The 1.00 mL, water injected into batch type reactor and gas circulation reactor, if all evaporated, could make the vapour concentration of 53040 ppmV and 112968 ppmV, theoretically. As not sure the lower water concentration measured in caused by water vapour was adsorbed by membrane or not all of water injected was vaporized, more water was injected in order to evaluate the effect of amount and timing of water injection.
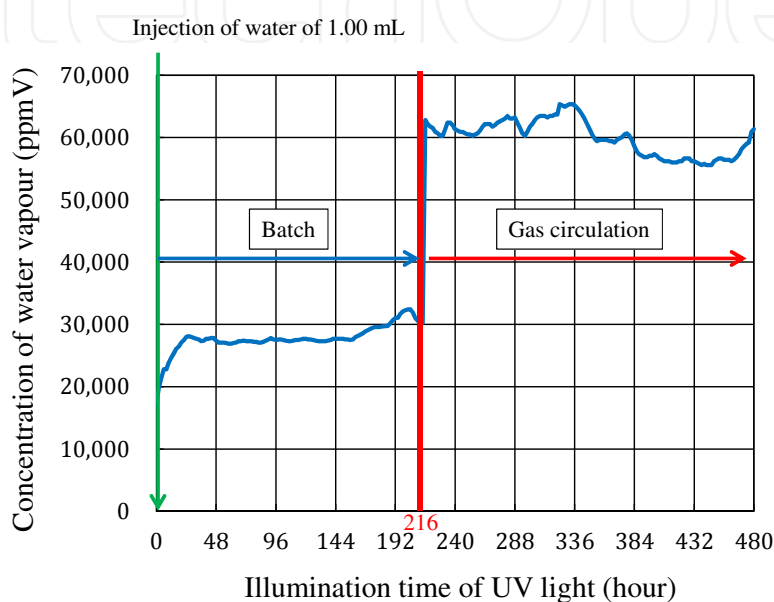
Fig. 18. Concentration change in water vapour during the CO$_2$ reforming experiment by batch type and gas circulation type reactor with illumination time of UV light (Injection of water of 1.00 mL at the start of CO$_2$ reforming experiment)

The further experiment plan was based on the assumption that at the steady and inverse reaction states, there was not sufficient water in the system. Therefore, the water was injected into CO$_2$ reformer when the steady and inverse reaction state in the CO$_2$ reforming was confirmed for not only batch type but also gas circulation type experiment. The amount of water injected was 1.00 mL at every time in this experiment. If the steady state was maintained after the injection of water in the batch type experiment by reactor, the gas circulation experiment then starts.

Figure 19 shows the concentration change in produced CO with illumination time of UV light. The initial distilled water of 1.00 mL (55.6 mmol) was injected into CO$_2$ reformer when the CO$_2$ reforming experiment by batch type reactor started. It had shown that the concentration of CO in the batch type reactor kept increasing until 168 h and the concentration of CO reached 136 ppmV. After the water of 1.00 mL was added into CO$_2$ reformer at 216 h when the steady state was confirmed, the concentration of CO increased again and attained to 186 ppmV at 480 h. Since the steady state was confirmed again at 504 h, another 1.00 mL of water was added into CO$_2$ reformer again. However, the concentration of CO did not increase any more, indicating the steady state maintained. After gas circulation started from 576 h, the concentration of CO started to increase again, and peaked

at 179 ppmV at total UV light illumination of 624 h. Since the steady state in the experiment by gas circulation type reactor was confirmed at 648 h, the further 1.00 mL of water was injected into $CO_2$ reformer. However, the concentration of CO did not increase further, indicating the water inside system was sufficient and its effect was peaked.
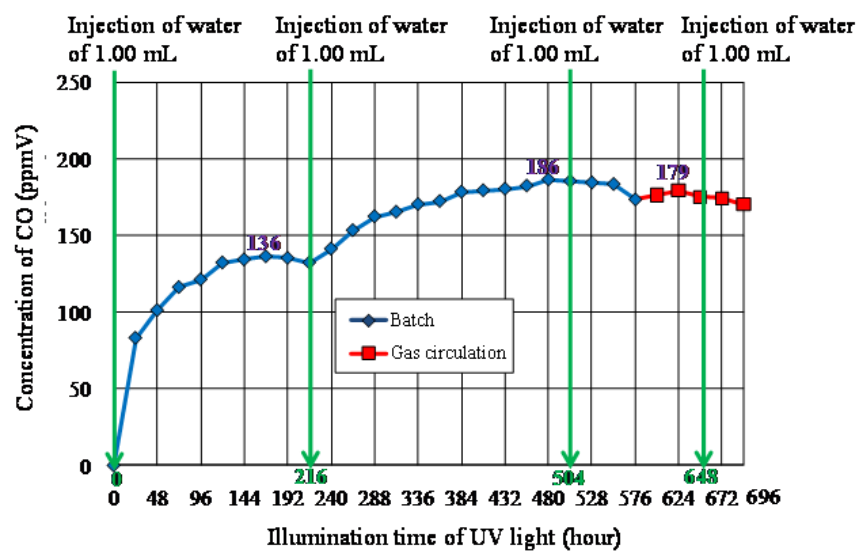


Fig. 19. Concentration change in produced CO with illumination time of UV light (Injection of water of 1.00 mL many times)

Figure 20 shows the concentration change in water vapour inside the system in the water adding experiment described above. From this figure, the measured concentration of water vapour obtained in $CO_2$ reforming experiment by batch type reactor is almost 25000 ppmV with total 3.00 mL water injected.
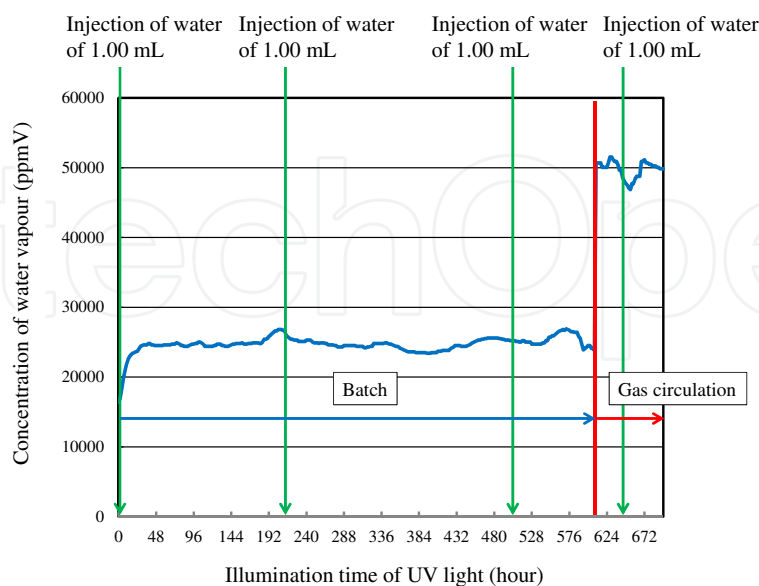


Fig. 20. Concentration change in water vapour during the $CO_2$ reforming experiment by batch type and gas circulation type reactor with illumination time of UV light (Injection of water of 1.00 mL many times)
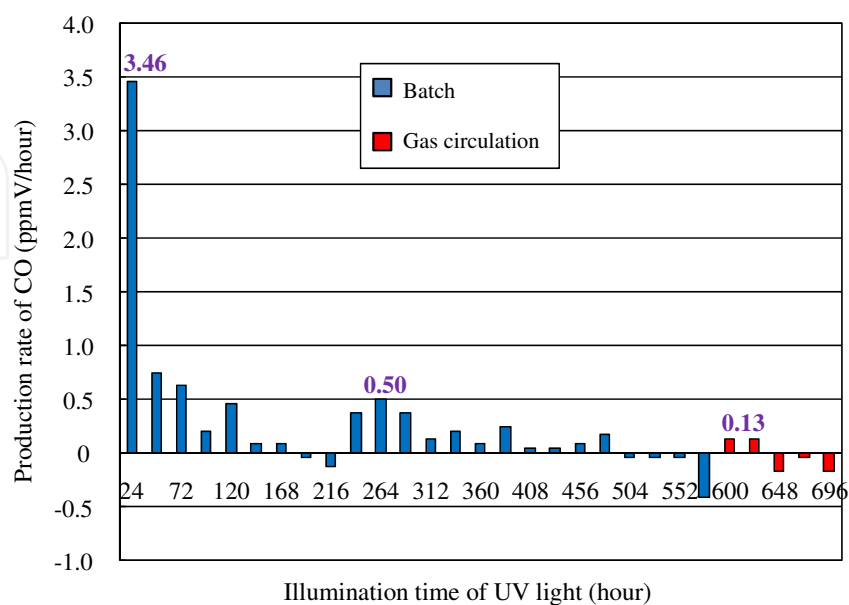
Fig. 21. Change in production rate of CO with illumination time of UV light (Injection of water of 1.00 mL many times)

Figure 21 shows the change in production rate of CO with illumination time of UV light. From this figure, it can be seen that there are two peaks of production rate of CO in CO$_2$ reforming experiment by batch type reactor, and there is one peak of production rate of CO in CO$_2$ reforming experiment by gas circulation type. The first peak was obtained at UV light illumination of 24 h with total of 1.00 mL water in the system, which was injected at the start of CO$_2$ reforming experiment. According to Fig.21, the production rate of CO decreases, after peaking at 24 h, gradually and reaches negative value at UV light illumination of 216 h. As mentioned above, since the steady reaction state was confirmed at UV light illumination of 216 h, the another 1.00 mL water was added into CO$_2$ reformer. As a result, the second peak was obtained at UV light illumination of 264 h. After that, the production rate of CO decreases again. Although further 1.00 mL water was added into CO$_2$ reformer again at UV light illumination of 504 h, the production rate of CO remains negative value. After gas circulation from total UV light illumination of 576 h, the production rate of CO increases and peaks at total UV light illumination of 600 h. From these results, the effect of water injection on the promotion of CO$_2$ reforming performance is verified. However, both the highest concentration and the highest production rate of CO in this CO$_2$ reforming experiment are lower than those in the case of only total 1.00 mL water injected. In addition, compared to the case of total amount of water injected of 1.00 mL, the effect of switching batch type reactor to gas circulation type reactor on the promotion of CO$_2$ reforming performance is not confirmed in this experiment.

Nevertheless the above described results seem reveals that the optimum timing of water injection is the very beginning of CO$_2$ reforming experiment. Therefore, one more

experiment was conducted, i.e. the distilled water of 3.00 mL (166.8 mmol) was injected into $CO_2$ reformer at the very beginning of the experiment. Figure 22 shows the concentration change in produced CO with illumination time of UV light. The experiment by batch type and gas circulation type reactor was carried out during the period from 0 h to 168 h and from 168 h to 264 h, respectively. The highest concentration of CO which is 126 ppmV is obtained at UV light illumination of 144 h. Since the concentration of CO is not increased over 144 h, indicating that the experiment by batch type reactor attains to the steady reaction state, the gas circulation was started. After gas circulation, the concentration of CO starts to increase again, and peaks at 171 ppmV at UV light illumination of 240 h.
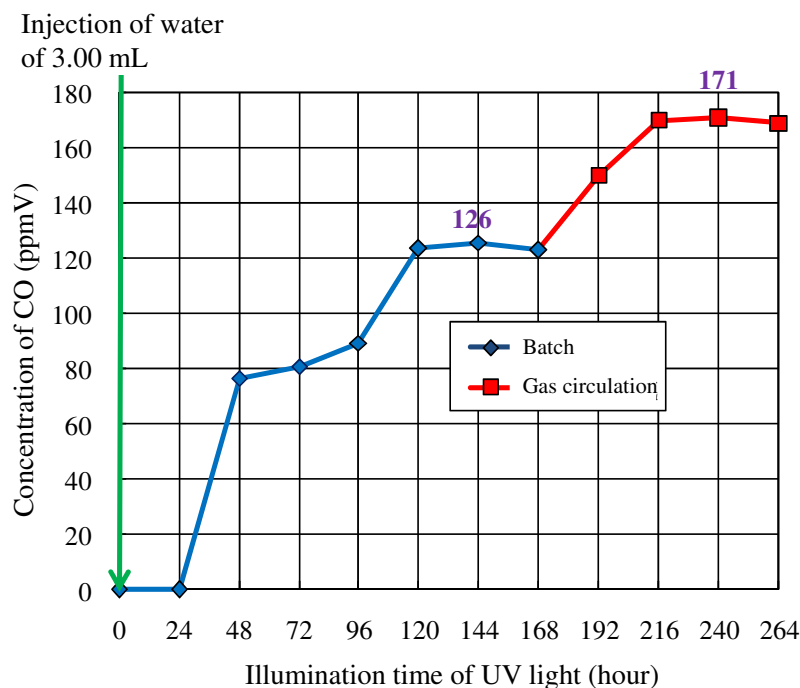
Fig. 22. Concentration change in produced CO with illumination time of UV light (Injection of water of 3.00 mL at the start of $CO_2$ reforming experiment)

Figures 23 and 24 show the comparison in production rate of CO and change rate of water vapour with illumination time of UV light for the amount of water injected of 1.00 mL and that of 3.00 mL, respectively. The change rate of water vapour which is calculated by Eq. (5):

$$R_{H_2O} = \frac{\Delta C_{H_2O}}{t_{int}}$$  (5)

where $R_{H_2O}$, $\Delta C_{H_2O}$ and $t_{int}$ means change rate of water vapour (ppmV/hour), the amount of increase in concentration of water vapour (ppmV) and measurement interval of water vapour (h), respectively. The used for calculating $R_{H_2O}$ is 24 h.
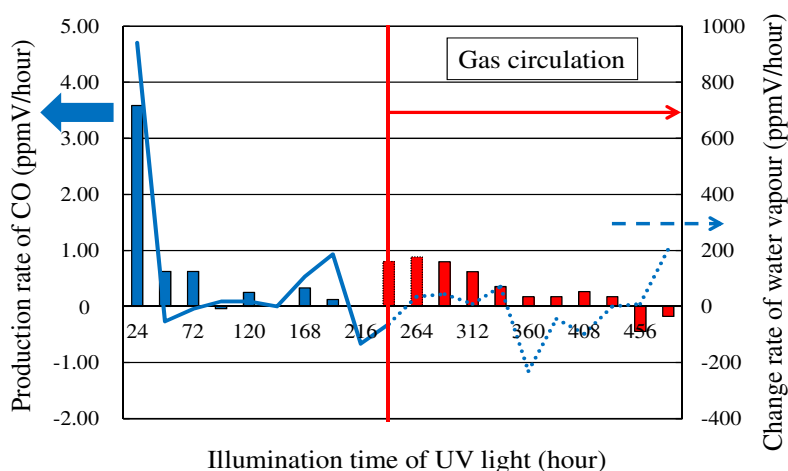
Fig. 23. Change in production rate of CO and change rate of water vapour with illumination time of UV light for the amount of water injected of 1.00 mL
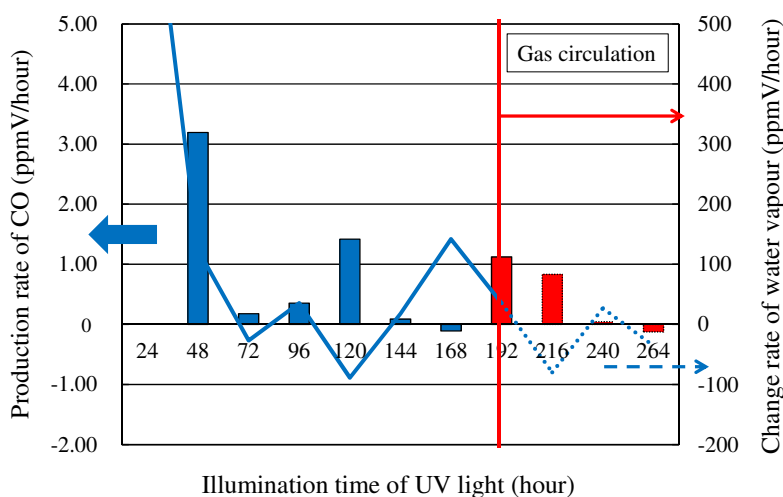


Fig. 24. Change in production rate of CO and change rate of water vapour with illumination time of UV light for the amount of water injected of 3.00 mL

From these figures, it can be seen that the concentration of water vapour in both cases, decreases rapidly from 0 h to 48 h. Since the highest production rates of CO for the amount of water injected of 1.00 mL and 3.00 mL are obtained from 0 h to 48 h, the $CO_2$ reforming is carried out well in the period. While the concentration of water vapour increases with illumination time of UV light from 0 h to 24 h due to temperature rise in $CO_2$ reformer, the change rate of water vapour closes to 0 in the period from 48 h to 96 h irrespective of the amount of water injected. Therefore, it can be thought that the amount of water consumed by photocatalytic reaction is balanced out by the amount of water vaporized due to the heat

of UV lamp in the period from 48 h to 96 h. After starting gas circulation, the change rate of water vapour keeps at low level and decreases gradually irrespective of the amount of water injected, while the production rate of CO rises. Since the $CO_2$ reforming performance is promoted by gas separation and circulation operation, the water vapour is consumed by the $CO_2$ reforming reaction. In addition, the water vapour is also adsorbed by drier, which is installed to protect the mass flow meter, in pipe line of gas circulation type reactor during gas circulation. The water concentration increase due to temperature increase is balanced out by both consumption by $CO_2$ reforming reaction and adsorption by drier. Therefore, the change rate of water vapour keeps low and decreases gradually after starting gas circulation. Consequently, it reveals that $CO_2$ reforming performance of gas circulation type reactor is declined by increasing the amount of water injected due to decreasing the concentration of water vapour.

Therefore, it can be concluded, too much water in that system, no matter when it was added, would not help improving the $CO_2$ reforming performance.

## 2.4 Proposal to establish the carbon circulation system using $TiO_2$ photocatalyst membrane reactor

As described above, the $CO_2$ reforming performance of $TiO_2$ photocatalsyt membrane reactor is still low. To enrich the product i.e. CO further, a hybrid system combining $TiO_2$ photocatalsyt membrane reactor with fuel concentrator is proposed as illustrated in Fig. 25.
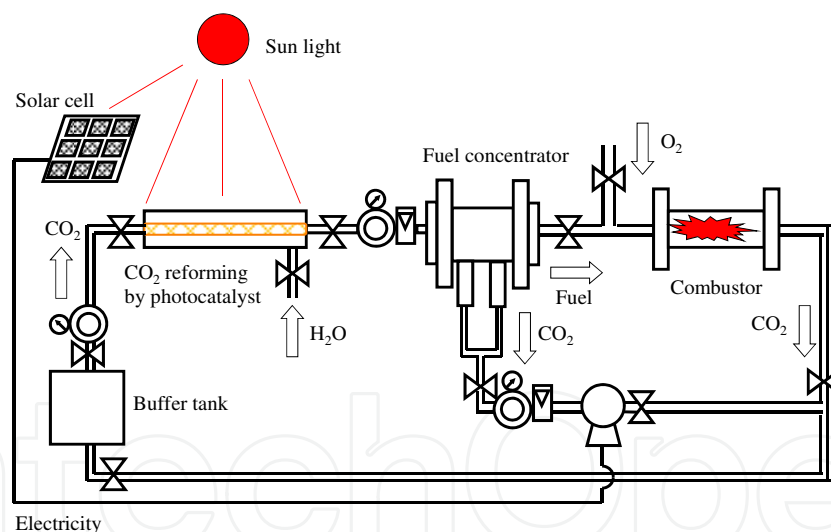


Fig. 25. Hybrid system combining $TiO_2$ photocatalyst membrane reactor with fuel concentrator

The fuel concentrator is a type of gas separation membrane. According to authors' previous study, the concentration of CO could be further enriched by the gas separation membrane which was composed of multiple hollow fibers. The concentration of CO of 3 vol.% in pre-mixed gas with $CO_2$, which simulated the maximum concentration of product by $CO_2$ reforming in the previous our studies, could be enriched by 6 times (Nishimura et al., 2007). If the pump necessary to enrich the fuel by the gas separation membrane as well as operating $TiO_2$ photocatalyst membrane reactor in the hybrid system can be powered by the

electricity generated by solar cell, and the photocatalytical reaction is powered by the sun light, the proposed hybrid system is a true power system with zero $CO_2$ emission.

## 3. Conclusion

This chapter introduces the recent research and development of the $TiO_2$ photocatalyst membrane reactor consisting of $TiO_2$ photocatalyst and gas separation membrane. The following conclusions were obtained.

i.   According to characterization by SEM, EPMA and XPS, the amount of $TiO_2$ film coated on gas separation membrane is reduced with increasing *RS*, and the largest amount of $TiO_2$ film is obtained for *RS* = 0.66 mm/s among various *RS* conditions investigated in this study.

ii.  According to $CO_2$ reforming experiment by batch type reactor, the concentration of CO is decreased with increasing *RS* gradually. On the other hand, the $CO_2$ permeation flux peaks at *RS* = 1.1 mm/s. Since the main goal of this study is to promote the $CO_2$ reforming performance, the *RS* = 0.66 mm/s is selected as the optimum coating condition in this study.

iii. According to $CO_2$ reforming experiment by gas circulation type reactor, the positive effect of gas separation and circulation on $CO_2$ reforming performance is confirmed. However, too much water in that system which can not be consumed in $CO_2$ reforming process, no matter when it was added, would not help improving the $CO_2$ reforming performance.

iv.  A concept power system with zero $CO_2$ emission, which consists of the $TiO_2$ photocatalsyt membrane reactor and fuel concentrator is proposed.

## 4. References

Adachi, K.; Ohta, K. & Mizuno, T. (1994). *Solar Energy*, Vol.53, No.2, pp.187-190

Anpo, M. & Chiba, K. (1992). *J. Mol. Catal.*, Vol.74, pp.207-212

Aurian-Blajeni, B.; Halmann, M. & Manassen, J. (1980). *Solar Energy*, Vol.25, pp.165-170

Cecchet, F.; Alebbi, M., Bignozzi, C. A. & Paolucci, F. (2006). *Inorg. Chim. Acta*, Vol.359, pp.3871-3874

Cueto, L. F.; Hirata, G. A. & Sanchez, E. M. (2006). *J. Sol-Gel Sci. Technol.*, Vol.37, pp.105-109

Dey, G. R.; Belapurkar, A. D. & Kishore, K. (2004). *J. Photochem. Photobiol. A : Chem.*, Vol.163, pp.503-508

Goren, Z.; Willner, I., Nelson, A. J. & Frank, A. J. (1990). *J. Phys. Chem.*, Vol.94, pp.3784-3790

Halmann, M.; Katzir, V., Borgarello, E. & Kiwi, J. (1984). *Solar Enregy Mater.*, Vol.10, pp.85-91

Henglein, A. & Gutierrez, M. (1983). *Ber. Bunsenges. Phys. Chem.*, Vol.87, pp.852-858

Hirano, K.; Inoue, K. & Yatsu T. (1992). *J. Photochem. Photobiol. A : Chem.*, Vol.64, pp.255-258

Ibusuki, T. (1993). *Syokubai*, Vol.35, pp.506-512

Inoue, T.; Fujishima, A., Konishi, S. & Honda, K. (1979). *Nature*, Vol.277, pp.637-638

Ishitani, O.; Inoue, C., Suzuki, Y. & Ibusuki, T. (1993). *J. Photochem. Photobiol. A : Chem.*, Vol.72, pp.269-271

Kaneco, S.; Kurimoto, H., Shimizu, Y., Ohta, K. & Mizuno, T. (1999). *Energy*, Vol.24, pp.21-30

Kawano, K.; Uehara, T., Kato, H. & Hirano, K. (1993). *Kagaku to Kyoiku*, Vol.41, pp.766-770

Lo, C. C.; Hung, C. H., Yuan, C. S. & Wu, J. F. (2007). *Solar Energy Mater. Solar Cells*, Vol.91, pp.1765-1774

Nakagawa, T. (1988). *Hyoumen*, Vol.26, No.7, pp.499-509

Nishimura, A.; Fujita, M. & Kato, S. (2007). *Proceedings of The 6th Asia Pacific Conference on Sustainable Energy and Environmental Technologies*, CD-ROM, Bangkok, Thailand, May 7-11, 2007

Ogura, K.; Kawano, M., Yano, J. & Sakata, Y. (1992). *J. Photochem. Photobiol. A. : Chem.*, Vol.66, pp.91-97

Ozcan, O.; Fukruk, F., Akkaya, E. U. & Uner, D. (2007). *Top. Catal.*, Vol.44, pp.523-528

Pathak, P.; Meziani, M. J., Li, Y., Cureton, L. T. & Sun, Y. P. (2004). *Chem. Commun.*, pp.1234-1235

Qu, J.; Zhang, X., Wang, Y. & Xie, C. (2005). *Elecrrochem. Acta 50*, pp.3576-3580

Takeuchi, K.; Murasawa, S. & Ibusuki, T. (2001). *World of Photocatalyst*, p.148, Kougyouchousakai, ISBN 4-7693-7063-6, Tokyo

Tseng, I. H.; Chang, W. C. & Wu, J. C. S. (2002). *Appl. Catal. B : Environ.*, Vol.37, pp.37-48

Wu, J. C. S. & Lin, H. M. (2005). *Int. J. Photoenergy*, Vol.7, pp.115-119

Xia, X. H.; Jia, Z. J., Yu, Y., Liang, Y., Wang, Z. & Ma, L. L. (2007). *Carbon*, Vol.45, pp.717-721

Yamashita, H.; Nishiguchi, H., Kamada, N. & Anpo, M. (1994). *Res. Chem. Intermed.*, Vol.20, pp.815-823
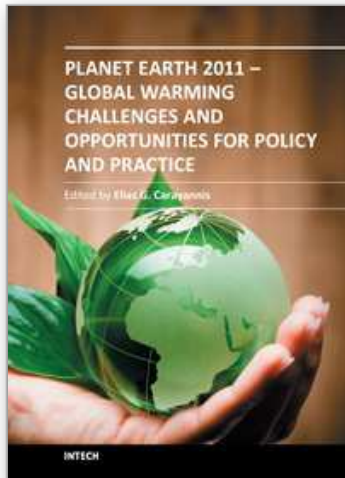
**Planet Earth 2011 - Global Warming Challenges and Opportunities for Policy and Practice**

Edited by Prof. Elias Carayannis

ISBN 978-953-307-733-8

Hard cover, 646 pages

**Publisher** InTech

**Published online** 30, September, 2011

**Published in print edition** September, 2011

The failure of the UN climate change summit in Copenhagen in December 2009 to effectively reach a global agreement on emission reduction targets, led many within the developing world to view this as a reversal of the Kyoto Protocol and an attempt by the developed nations to shirk out of their responsibility for climate change. The issue of global warming has been at the top of the political agenda for a number of years and has become even more pressing with the rapid industrialization taking place in China and India. This book looks at the effects of climate change throughout different regions of the world and discusses to what extent cleantech and environmental initiatives such as the destruction of fluorinated greenhouse gases, biofuels, and the role of plant breeding and biotechnology. The book concludes with an insight into the socio-religious impact that global warming has, citing Christianity and Islam.

**How to reference**

In order to correctly reference this scholarly work, feel free to copy and paste the following:

Akira Nishimura and Eric Hu (2011). Reforming CO2 into Fuel Using a TiO2 Photocatalyst Membrane Reactor, Planet Earth 2011 - Global Warming Challenges and Opportunities for Policy and Practice, Prof. Elias Carayannis (Ed.), ISBN: 978-953-307-733-8, InTech, Available from: http://www.intechopen.com/books/planet-earth-2011-global-warming-challenges-and-opportunities-for-policy-and-practice/reforming-co2-into-fuel-using-a-tio2-photocatalyst-membrane-reactor

# INTECH
open science | open minds